Chemical Science

ROYAL SOCIETY OF CHEMISTRY

EDGE ARTICLE

View Article Online
View Journal | View Issue

Cite this: *Chem. Sci.*, 2024, **15**, 12431

All publication charges for this article have been paid for by the Royal Society of Chemistry

Received 22nd March 2024
Accepted 10th June 2024

DOI: 10.1039/d4sc01915f

rsc.li/chemical-science

A *de novo* zwitterionic strategy of ultra-stable chemiluminescent probes: highly selective sensing of singlet oxygen in FDA-approved phototherapy†

Yao Lu,‡[a] Yutao Zhang,‡[a] Xia Wu,[b] Ruihua Pu,[c] Chenxu Yan,[a] Weimin Liu,[c] Xiaogang Liu,[b] Zhiqian Guo*[a] and Wei-Hong Zhu[a]

Singlet oxygen ($^1O_2$), as a fundamental hallmark in photodynamic therapy (PDT), enables ground-breaking clinical treatment in ablating tumors and killing germs. However, accurate *in vivo* monitoring of $^1O_2$ remains a significant challenge in probe design, with primary difficulties arising from inherent photo-induced side reactions with poor selectivity. Herein, we report a generalizable zwitterionic strategy for ultra-stable near-infrared (NIR) chemiluminescent probes that ensure a highly specific [2 + 2] cycloaddition between fragile electron-rich enolether units and $^1O_2$ in both cellular and dynamic *in vivo* domains. Innovatively, zwitterionic chemiluminescence (CL) probes undergo a conversion into an inert ketone excited state with an extremely short lifetime through conical intersection (CI), thereby affording sufficient photostability and suppressing undesired photoreactions. Remarkably, compared with the well-known commercial $^1O_2$ probe SOSG, the zwitterionic probe QMI exhibited an ultra-high signal-to-noise ratio (SNR, over 40-fold). Of particular significance is that the zwitterionic CL probes demonstrate excellent selectivity, high sensitivity, and outstanding photostability, thereby making a breakthrough in real-time tracking of the FDA-approved 5-ALA-mediated *in vivo* PDT process in living mice. This innovative zwitterionic strategy paves a new pathway for high-performance NIR chemiluminescent probes and high-fidelity feedback on $^1O_2$ for future biological and medical applications.

Introduction

Singlet oxygen ($^1O_2$), a highly reactive oxygen species (ROS), has the remarkable capacity to induce oxidative stress in cells.[1–3] This striking property of $^1O_2$ has enabled ground-breaking clinical treatments for ablating tumors and killing germs.[4–10] The quantification of $^1O_2$ in photodynamic therapy (PDT) is the dominant feature as a dependable gauge of therapeutic effect, which not only bestows immediate feedback on treatment but also confers optimal therapy protocols.[11,12] However, the progress in monitoring cellular $^1O_2$ has been seriously impeded by the inability to extrapolate an effective solution for the probe. The exceedingly short lifetime of $^1O_2$ (<1 μs),[13] coupled with interference from other ROS in tumor tissues,[14] makes it extremely difficult to precise $^1O_2$ detection across both cellular and dynamic *in vivo* domains. To date, the gold standard for $^1O_2$ determination relies upon the rigorous instrument for feeble phosphorescence signals at 1270 nm and thereby is merely utilized for *in vitro* application.[15] Hence, there is an urgent demand to develop a design strategy for highly sensitive and selective probes for the *in vivo* detection of singlet oxygen.

The features of optical probes hold great potential for revolutionizing the accurate *in vivo* detection of singlet oxygen.[16–21] In general, current $^1O_2$ probes predominantly rely on strong oxidative reactions, thereby inability to discriminate $^1O_2$ from stronger oxidative ROS species, such as commercial 9,10-anthracenediyl-bis(methylene)-dimalonic acid (ABDA).[22] Most importantly, the contradiction between an undesirable photo-induced reaction and imperative light irradiation makes it seriously difficult to search for an effective solution for the *in vivo* $^1O_2$ probe (Fig. 1A). For instance, the well-known Singlet Oxygen Sensor Green (SOSG, a commercial probe) suffers from its self-sensitization, leading to inevitable overestimations of $^1O_2$.[23–25] Indeed, the [2 + 2] cycloaddition reactions between the enolether and $^1O_2$ in chemiluminescence (CL) provide an effective solution to discriminate $^1O_2$ from other ROS,[26–29] but the highly electron-rich enolether moiety is generally fragile

[a]*Key Laboratory for Advanced Materials, Institute of Fine Chemicals, Feringa Nobel Prize Scientist Joint Research Center, Frontiers Science Center for Materiobiology and Dynamic Chemistry, School of Chemistry and Molecular Engineering, East China University of Science and Technology, Shanghai 200237, China. E-mail: guozq@ecust.edu.cn*

[b]*Fluorescence Research Group, Singapore University of Technology and Design, 8 Somapah Road, Singapore, 487372, Singapore*

[c]*School of Physical Science and Technology, ShanghaiTech University, Shanghai 201210, China*

† Electronic supplementary information (ESI) available. See DOI: https://doi.org/10.1039/d4sc01915f

‡ Y. L. and Y. Z. contributed equally to this work.

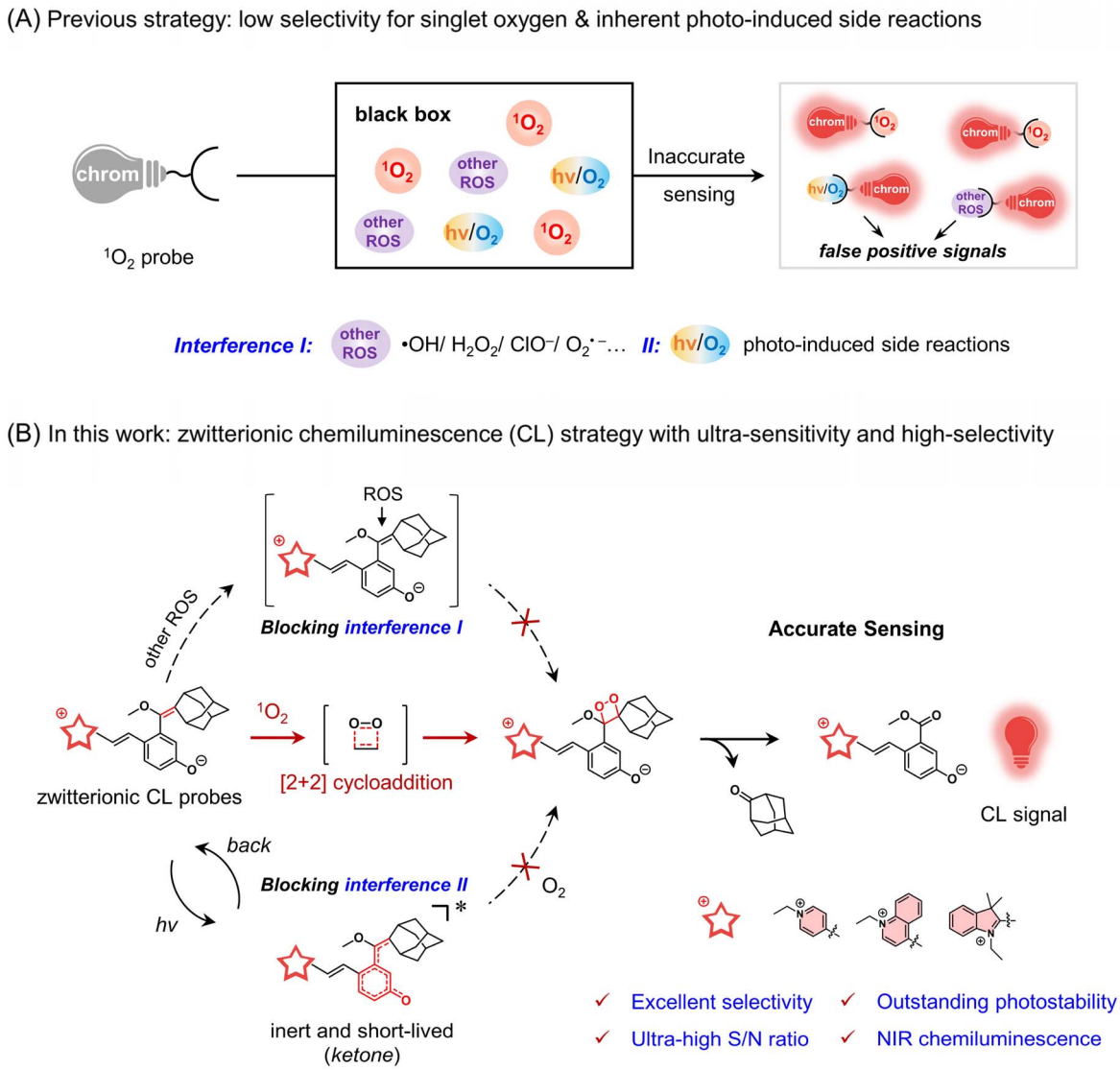

Fig. 1 Zwitterionic chemiluminescence (CL) strategy enables accurate sensing of $^1O_2$. (A) Previous optical probes for sensing $^1O_2$ with low selectivity and photo-induced side reactions inevitably produce misleading responses. (B) In our strategy, zwitterionic ultra-stable CL probes for accurately sensing $^1O_2$ are specifically triggered by the [2 + 2] cycloaddition reaction between the enolether moiety and $^1O_2$; the generation of inert and short-lived ketone excited states of zwitterionic probes enables the effective suppression of photo-induced side reactions.

under light irradiation,[30–32] thereby inevitably leading to undesirable photo-induced side reactions.[33,34] Furthermore, near-infrared chemiluminescent emission is essential to improving tissue *in vivo* penetration.[35–38] Thus, the elaborate strategy of converting photo-active electron-rich enolether into a photo-inert state would make a breakthrough in $^1O_2$ probe solution for ultra-stable NIR chemiluminescent probes.

Herein, we present an innovative zwitterionic strategy to construct ultra-stable NIR chemiluminescent probes, which covalently bridge cationic chromophores with a phenolic dioxetane precursor *via* a short methine chain (Fig. 1B). The unique zwitterionic configuration endows the probes with the following key features: Firstly, the "merocyanine configuration" extends the luminescence of these probes into the NIR region. Secondly, the highly specific [2 + 2] cycloaddition reaction of the enolether moiety in the probe with $^1O_2$ endows excellent selectivity. The subsequent cycloadducts producing bright chemiluminescence ensure the ultra-high sensitivity of the probes towards $^1O_2$. Thirdly, most importantly, the photo-inert ketone excited state of the zwitterionic probe, coupled with its extremely short excited-state lifetime, could effectively mitigate undesired photo-induced side reactions. Compared to the reported CL probes and commercial SOSG, these zwitterionic probes exhibit remarkable photostability and superior sensitivity towards $^1O_2$. Notably, for the first time, utilizing the ultra-stable zwitterionic CL probes allows us to accurately *in vivo* monitor $^1O_2$ from the FDA-approved 5-aminolevulinic acid (5-ALA)-mediated PDT process in living mice. This zwitterionic ultra-stable CL strategy opens avenues for a new type of *in vivo* $^1O_2$ probe.

Results and discussions

Exploring the zwitterionic design strategy for CL probes

As mentioned, insufficient selectivity, low sensitivity, and inherent photo-induced side reactions become the bottlenecks for $^1O_2$ optical probes. In addressing these challenges, the enolether unit, a recognized chemiluminescent building block that imparts chemical energy by the specific [2 + 2] cycloaddition reaction with $^1O_2$,[39–41] was employed as a specific recognition unit for $^1O_2$. However, constrained by the electron-rich nature of the enolether unit, these chemiluminophores are prone to photo-oxidation reactions under light irradiation, leading to undesirable photodegradation and photo-induced CL signals.

To address this dilemma between structural requirements and photostability, we turn our attention to merocyanine with zwitterionic and quinoid forms, which possess the distinctive feature of conical intersection (CI) between the ground and excited-state potential energy surfaces.[42] The presence of CI could greatly shorten the excited-state lifetime of merocyanine, thereby effectively suppressing self-oxidation reactions. Consequently, we engineered three zwitterionic CL probes (PyCL, QMI, and InCL) featuring "merocyanine configuration" by bridging three cationic chromophores (*N*-ethylpyridine, *N*-ethylquinoline, and *N*-ethylindole) with the phenolic luminophore containing enolether at the para position, respectively (Fig. 2A and Scheme S1†). We anticipated that the zwitterionic probes would exhibit significant photostability under light irradiation, thus maintaining a photo-inert response in the chemiluminescent channel.

As shown in Fig. 2B, the CL signals of DCMCL and QMCL were observed with 181-fold and 46-fold enhancement under light irradiation, respectively. It was suggested that this enhancement should be ascribed to the photooxidation reaction. Furthermore, after light irradiation for 21 min, high-performance liquid chromatography (HPLC) experiments revealed that QMCL underwent rapid photodegradation, with up to a 99.4% degradation rate. It is noteworthy that the retention time of the decomposition product was merely 2.27 min, presumably due to the removal of the adamantane substituent (Fig. 2C and F). Similar fast decomposition was also found in the probe DCMCL (Fig. 2F and S1†).

Revealing ultra-stable and highly selective characteristics of zwitterionic CL probes towards singlet oxygen

For three zwitterionic probes (PyCL, QMI, and InCL), there were only neglectable CL signal changes under light irradiation (Fig. 2D), indicating the zwitterionic strategy is beneficial for the improvement of ultra-stability. Specifically, QMI displayed excellent photostability under the same light irradiation as QMCL (Fig. 2E and F). Moreover, high-resolution mass spectrometry (HRMS) further confirmed the decomposition process, which was produced in the chemiluminescent process under light irradiation (Fig. S1–S3†). In addition, the compared experiments of QMCL and zwitterionic CL probes in a mixture of PBS/DMSO with different PBS fractions (f_w) verified that the zwitterionic CL probes have sufficient stability under light irradiation (Fig. S4 and S5†). Clearly, these zwitterionic CL probes ensure a significantly stable electron-rich enolether moiety, resulting in minimized photo-induced side effects with outstanding photostability.

Next, we investigated the photophysical properties of the designed zwitterionic CL probes. Obviously, compared with PyCL and InCL, the probe QMI has a longer emission, thereby making it better suitable for *in vivo* applications (Fig. S6 and S7†). Therefore, we chose QMI as a model for the accurate detection of $^1O_2$ *in vivo*. In fact, the pK_a value (pK_a = 6.8) implied that QMI was susceptible to deprotonation at the physiological pH condition (Fig. S8†). Similar to negative-solvatochromic dyes,[43] QMI tends to perform an amphoteric configuration in a large polar solvent such as water (Fig. S9†). Then, the CL spectrum of QMI was observed extending into the NIR region (emission peak at 680 nm), which is suitable for *in vivo* applications (Fig. 2G).[44]

The selectivity of QMI toward reactive oxygen species (ROS) was carried out. As expected, only QMI towards $^1O_2$ emits a remarkably enhanced CL signal, while other ROS or only light irradiation produce negligible responses (Fig. 2H). It means that the CL signal from QMI could only be specifically activated in the presence of $^1O_2$. Collectively, our simple and generalizable zwitterionic design strategy endows CL probes with ultra-stability and excellent selectivity for $^1O_2$ over other potential ROS.

Discovering the conical intersection mechanism of zwitterionic CL probes

Very recently, we demonstrated that the CL probes bring about reactive radical species under photoexcitation and then react with oxygen to generate 1,2-dioxetane, thereby initiating light-induced CL signals.[34] Thus, we reasonably believed that the zwitterionic probes should manifest distinct photoexcited states to intercept reactions in the presence of oxygen (Fig. 3A). The remarkable photostability of zwitterionic probes motivates us to gain further insight into their intrinsic mechanism by utilizing time-dependent density functional theory (TD-DFT) calculations and femtosecond transient absorption spectroscopy (fs-TAS).

TD-DFT calculation results indicated that QMCL (photoactivatable CL probe) has a small energy barrier (0.02 eV) and possesses a considerable driven force (0.79 eV), thereby entering the twisted intramolecular charge transfer (TICT) states upon photoexcitation (Fig. 3B). Simultaneously, the corresponding oscillator strength (*f*) decreased to zero, and a total charge separation was observed between the donor and acceptor fragments in the TICT state (Fig. S10†). Notably, the large optical gap (between the S_1 and S_0 states, 0.39 eV) of QMCL makes its TICT state have a long lifetime (the energy gap law). Consequently, the complete charge separation in the TICT state led to the formation of radical compounds. Thus, the highly reactive and long-lived TICT state ensured that QMCL reacted with oxygen to form 1,2-dioxetane, triggering subsequent chemiluminescence (Fig. 3A).

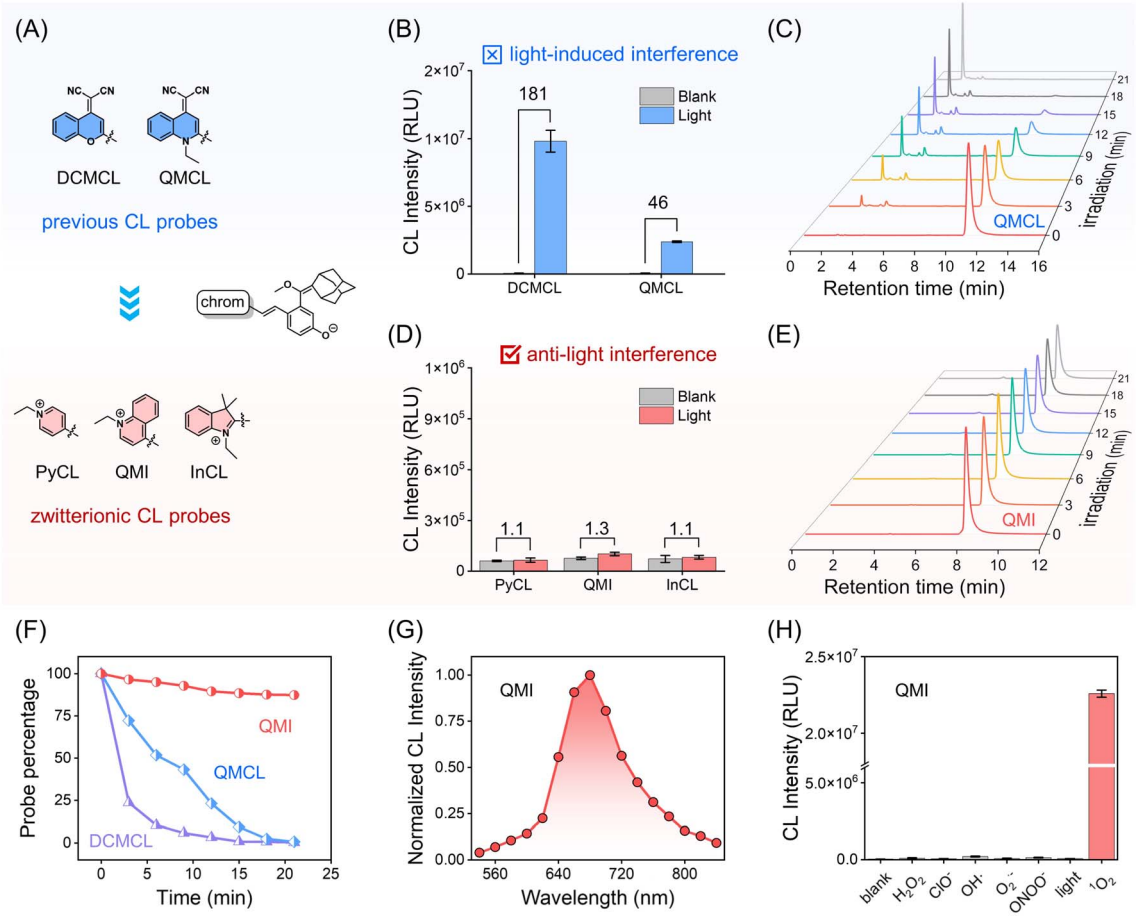

Fig. 2 Construction of ultra-stable and highly selective chemiluminescent probes for singlet oxygen based on a zwitterionic strategy. (A) Chemical structures of previous and zwitterionic CL probes. (B) The light-induced interference of previous CL probes with potential photo-oxidation reaction upon white light (120 mW cm^{-2}) irradiation for 1 min. (C) Time-resolved HPLC profiles of QMCL under light irradiation (white light, 1.6 W cm^{-2}; bubbling oxygen into the solution). (D) Anti-light interference of zwitterionic CL probes with outstanding photostability upon white light (120 mW cm^{-2}) irradiation for 1 min. (E) Time-resolved HPLC profiles of QMI under the same test conditions as (C). (F) Quantification of DCMCL, QMCL, and QMI with light irradiation in HPLC. (G) Chemiluminescence spectrum of QMI. (H) CL signal intensity of QMI (50 μM) towards $^1O_2$ (produced by 10 μM methylene blue), light irradiation (2 min), and other ROS (50 equiv.) in PBS buffer solution. Data with error bars are expressed as mean ± s.d., $n = 3$.

In contrast, TD-DFT calculation results for QMI revealed the occurrence of a conical intersection (CI) between the S_1 and S_0 states, so that the photochemical reaction between QMI and oxygen was efficiently inhibited. Specifically, as θ rotates from 0° to 90° to enter the TICT state of QMI (Fig. S10†), the optical gap (between the S_1 and S_0 states) quickly approaches zero, thereby resulting in a conical intersection (CI) between the S_1 and S_0 states (Fig. 3C). It should be noted that CI serves as a rapid non-radiative decay channel and leads to an extremely short-lived excited state.[45,46] Furthermore, the smaller dipole moment (μ = 23.574 D) and the shorter C–O bond length (1.252 Å) of QMI (Fig. S11 and Table S1†) verified that the electron transfer from the phenoxy anion to the positively charged nitrogen atom brings QMI into the inert ketone form. Similar calculation results were also observed in the zwitterionic PyCL and InCL (Fig. S12 and S13†). Clearly, due to the formation of inert and short-lived excited species, these zwitterionic probes do not generate chemiluminescence upon light irradiation, thereby showing the ultra-stable characteristic.

Then, the fs-TAS was employed to validate the excited-state dynamics of QMI.[47,48] Transient absorption spectra showed that QMI had a significantly shorter excited-state lifetime than that of QMCL and DCMCL (Fig. 3D, E and S14†). The stimulated emission at 720 nm was selected as a representative band to evaluate the excited-state lifetimes of the three compounds. As shown in Fig. 3F, the stimulated emission signal of QMI at 720 nm decayed rapidly, with a lifetime of 14 ps. In contrast, the stimulated emission decay of QMCL and DCMCL at 720 nm became significantly slower, with lifetimes of 62 ps and 80 ps, respectively. Moreover, in water solution, the stimulated emission lifetime of QMI was even shortened to 7 ps (Fig. S15†). Furthermore, the transient absorption spectra of QMI in acetonitrile solution provide solid evidence for the CI mechanism proposed in the TD-DFT calculations, which is consistent with the results for merocyanine in previous studies (Fig. S16†).[46] All of these calculation results and experimental data agree with our design principle for ultra-stable and high-selective zwitterionic CL probes, that is, the generation of

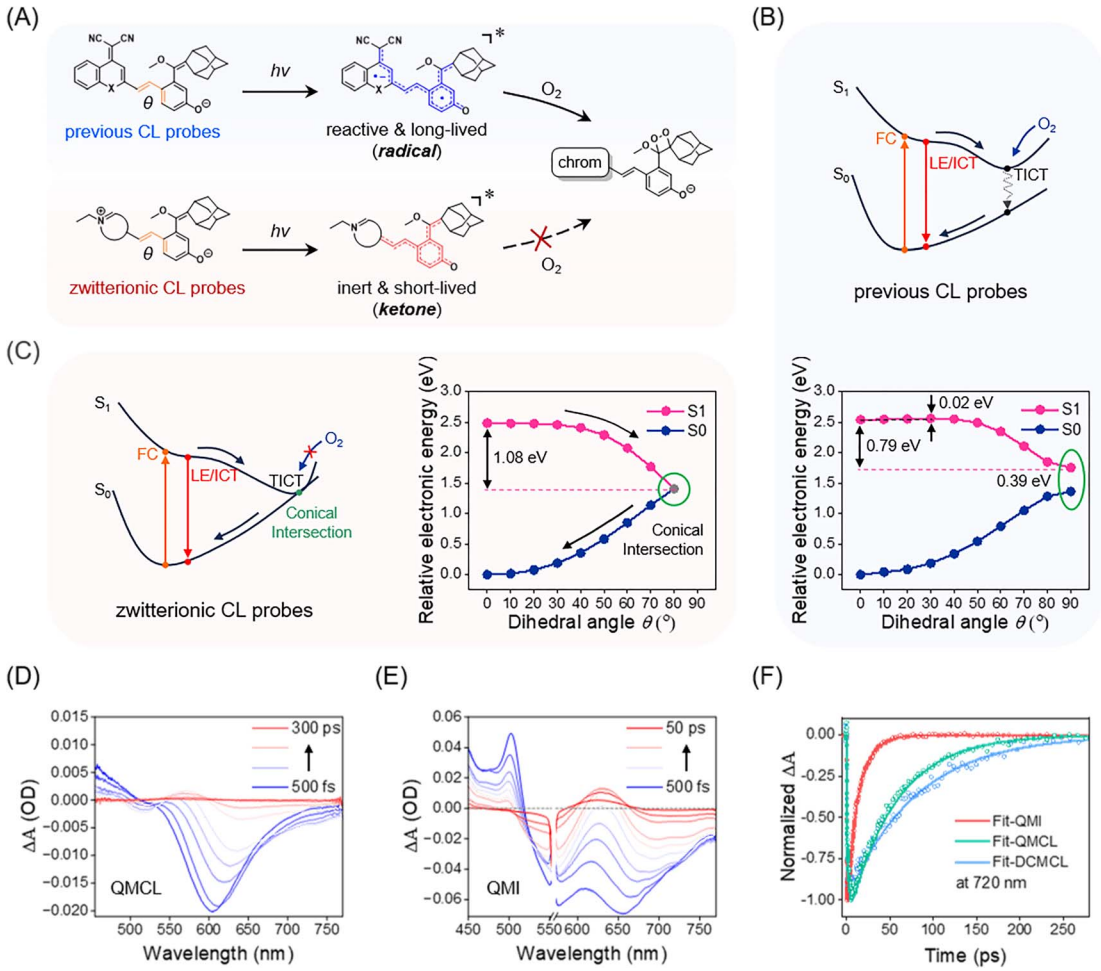

Fig. 3 Insight into the conical intersection mechanism of zwitterionic probes to suppress photo-induced side reactions. (A) Previous CL probes become reactive and long-lived radical species upon photoexcitation, and then react with oxygen to form 1,2-dioxetane; zwitterionic CL probes turn into inert and short-lived ketone excited states upon photoexcitation and then rapidly return to ground states, thus suppressing photoreaction with oxygen. (B) Schematic illustration of previous CL probes. S_1 (pink) and S_0 (dark blue) potential energy surfaces of QMCL as a function of rotating angle (θ). Note: the dihedral angle (θ) is highlighted in orange in Fig. 3A. (C) Schematic illustration of ultra-stable zwitterionic CL probes. S_1 (pink) and S_0 (dark blue) potential energy surfaces of QMI as a function of rotating angle (θ). Transient absorption spectra of (D) QMCL (100 μM, $\lambda_{ex} = 450$ nm) and (E) QMI (100 μM, $\lambda_{ex} = 560$ nm) were obtained in a mixture of PBS/DMSO (v/v = 1/1). Note: in Fig. 3D, lines indicate transient absorption spectra at 500 fs, and 1, 2.5, 5, 10, 50, 100, 200, and 300 ps. In Fig. 3E, lines indicate transient absorption spectra at 500 fs, and 1, 2, 3, 5, 7.5, 10, 20, 30, and 50 ps. (F) Kinetic traces of QMI, QMCL, and DCMCL at 720 nm. The solid lines are the fitting curves with a multiexponential decay function.

short-lived and inert ketone excited species impedes the potential undesirable photoreaction, thereby effectively eliminating the interference from photo-induced side reactions.

Verifying high-performance zwitterionic CL probes toward singlet oxygen over commercial probe SOSG

It still remains critical and challenging to track transient $^1O_2$ with sufficient sensitivity in living organisms.[49,50] We investigated whether the zwitterionic CL probe QMI could meet the demand for $^1O_2$ for efficient signal transduction. As shown in Fig. 4A, through the [2 + 2] cycloaddition reaction, the electron-rich enolether specifically traps $^1O_2$ to generate an unstable high-energy 1,2-dioxetane structure, and subsequent decomposition of the 1,2-dioxetane leads to NIR emission. This mechanism was confirmed by HPLC-MS analysis (Fig. S17 and S18†). It is worth noting that there was no significant change in the fluorescence emission spectra of QMI before and after the reaction with $^1O_2$ (Fig. S19†), making it difficult to trace $^1O_2$ by fluorescence. Based on this activated process, we evaluated the capability of QMI for sensing $^1O_2$ produced by methylene blue (MB), a widely utilized photosensitizer (PS) for PDT of solid tumors. As expected, QMI exhibited a remarkable CL signal in response to $^1O_2$ from MB under light irradiation, achieving an ultra-high S/N ratio (approximately 488-fold) (Fig. S20†) with a typical glow-type CL kinetic profile. In contrast, no CL signal was observed from QMI without light irradiation. The fact that the CL intensity increased linearly with the light irradiation time provided ultra-sensitive feedback on $^1O_2$ generation by the photosensitizer MB. In addition, for other commercial photosensitizers such as rose bengal (RB) and porphyrins (chlorin e6,

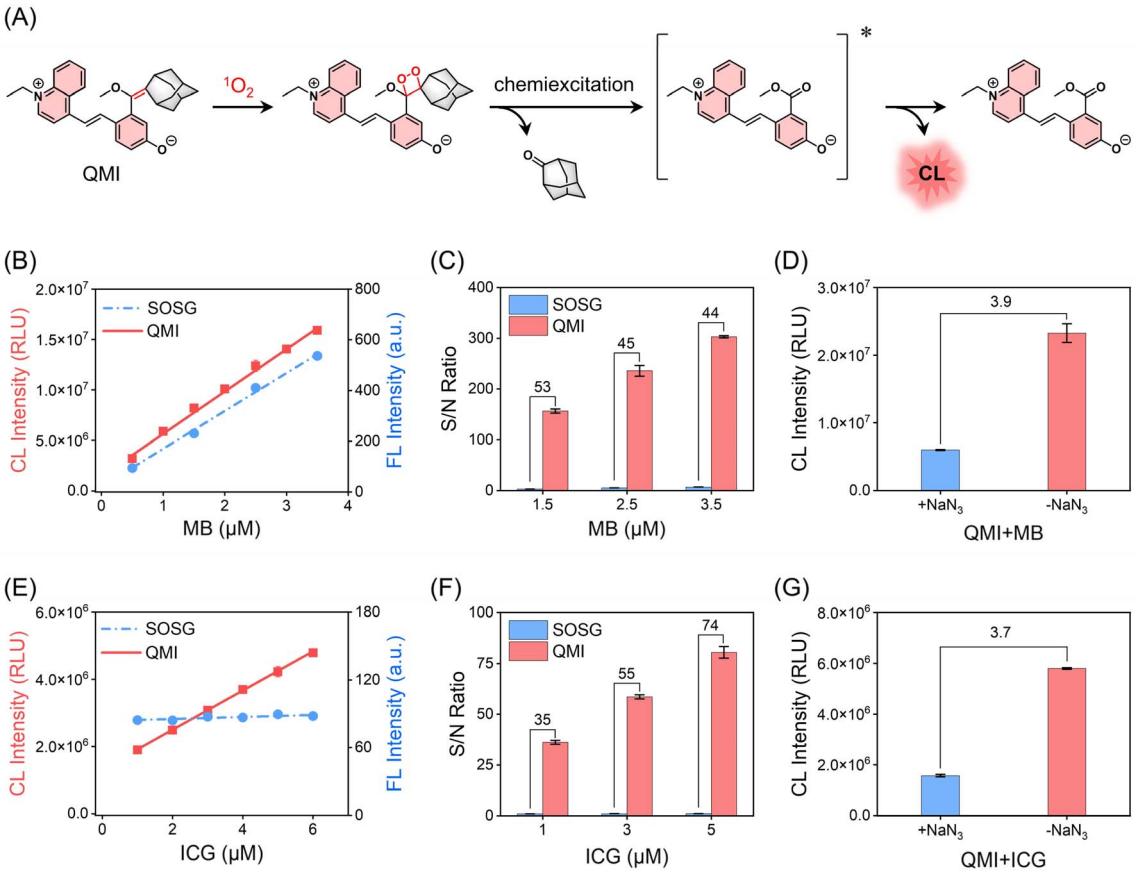

Fig. 4 Zwitterionic CL probes enable ultra-sensitive detection of singlet oxygen. (A) Sensing mechanism of QMI as the $^1O_2$ probe. Linear correlation between signal intensities of QMI/SOSG and concentrations of MB (B) or ICG (E). Comparison of the S/N ratios of QMI and SOSG at different concentrations of MB (C) or ICG (F). CL signal intensities of QMI + MB (D) and QMI + ICG (G) with NaN_3 ($^1O_2$ scavenger, 1 mM). MB experiment: the mixed solution was exposed to a 690 nm laser (200 mW cm^{-2}) for 1 min. ICG experiment: the mixed solution was exposed to an 808 nm laser (200 mW cm^{-2}) for 3 min. Data with error bars are expressed as mean ± s.d., $n = 3$.

Ce6; hematoporphyrin monomethyl ether, HMME; protoporphyrin IX, PpIX), we also observed similar properties. Importantly, the CL signal intensity of QMI displayed an excellent linear relationship with the concentration of these photosensitizers (Fig. S21†). This observation underscored its capacity for accurately detecting the level of $^1O_2$ produced by the photosensitizers.

To demonstrate the ultra-sensitivity of QMI towards $^1O_2$, two well-known commercial $^1O_2$ probes, ABDA and SOSG, were selected as references. Herein, for the contrast experiments, photosensitizer MB was chosen as a typically efficient $^1O_2$ generator. As shown in Fig. 4B, there was a good linear correlation ($R^2 = 0.996$) between the CL intensity of QMI and the concentration of MB, indicating that the $^1O_2$ generated by MB can be intuitively detected and quantified by CL signal changes. Similarly, commercial probe SOSG based on fluorescent changes was observed for the detection of $^1O_2$ generated from MB. It was noteworthy that QMI had a significantly lower limit of detection (LOD) for $^1O_2$ in comparison to SOSG ($LOD_{QMI} = 4.3$ nM, $LOD_{SOSG} = 42.4$ nM). Especially, the S/N ratio (SNR) of QMI towards $^1O_2$ was much higher than that of SOSG at the various concentrations of MB (Fig. 4C). Additionally, SOSG has the propensity to self-sensitize, thus producing unexpected additional $^1O_2$ under light irradiation. This inherent characteristic of SOSG inevitably gives rise to false positive signals, thereby providing misleading information (Fig. S22†). Another commercial probe, ABDA, based on absorbance intensity changes, displayed the lowest SNR under the same condition (Fig. S23†). Furthermore, the introduction of NaN_3 ($^1O_2$-specific scavenger) led to a substantial 74% decrease in the CL intensity of QMI (Fig. 4D), serving as robust evidence that the specific [2 + 2] cycloaddition reaction between QMI and $^1O_2$ initiated the CL signal change.

To further assess the sensitivity of zwitterionic probes for $^1O_2$, we evaluated the capability of QMI to detect and trace the low-efficiency photosensitizers during PDT. Indocyanine green (ICG), an FDA-approved clinical reagent, was selected as a representative of low-efficiency photosensitizers, and was documented for PDT as early as 20 years ago.[51,52] The photosensitive efficiency of ICG is *ca.* 7.7%, and it is difficult to be recognized by traditional probes due to its self-consumption of $^1O_2$.[53–55] Excitingly, QMI demonstrated a quantitative response to even subtle $^1O_2$ produced by ICG (1 μM), achieving an impressive 35-fold SNR with a LOD as low as 30.9 nM (Fig. 4E

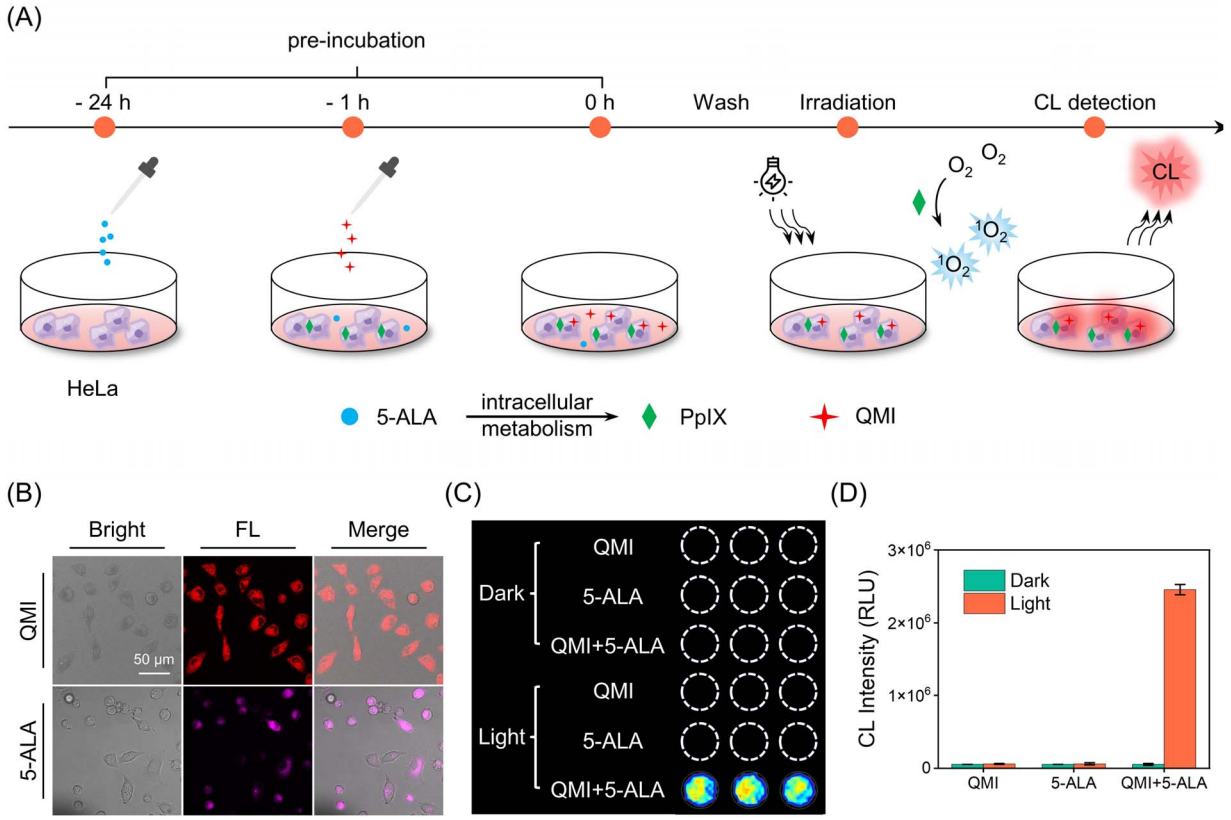

Fig. 5 Lighting up endogenous $^1O_2$ from FDA-approved 5-ALA phototherapy in living cells. (A) Schematic illustration of cell treatment and imaging procedure. (B) Confocal fluorescent images of HeLa cells incubated with QMI (10 μM) for 1 h and 5-ALA (1 mM, PpIX precursor) for 24 h, respectively. QMI group excitation at 520 nm and collection at 600–700 nm; 5-ALA group excitation at 410 nm and collection at 620–710 nm. Scale bar = 50 μm. (C) HeLa cells were incubated with QMI (20 μM), 5-ALA (1 mM) alone, or 5-ALA followed by QMI, and then the CL images were obtained with or without 635 nm laser (200 mW cm^{-2}) irradiation for 3 min. (D) Quantification of CL intensity emitted from the HeLa cells. Data with error bars are expressed as mean ± s.d., $n = 3$.

and F). In contrast, under the same condition, there was negligible signal change for SOSG and ABDA, respectively (Fig. 4E and S23†). Following the addition of NaN_3, the CL signal intensity of QMI decreased to 27% of the initial CL intensity, confirming that ICG sensitizes oxygen to produce certain $^1O_2$ under light irradiation (Fig. 4G). In addition, the CL signal of QMI increased continuously with the extension of irradiation time at a given ICG concentration (Fig. S24†). Importantly, similar results for sensing $^1O_2$ were also observed in the pentamethine cyanine dyes (Cy5) (Fig. S25†). Taken together, these results highlighted the remarkable advantages of QMI in terms of detection sensitivity and contrast ratio over commercial probes.

Lighting up endogenous singlet oxygen in living cells

The ultra-high sensitivity, excellent selectivity, and outstanding photostability of this zwitterionic CL probe QMI encouraged us to further evaluate its capability for intracellular $^1O_2$. The cytotoxicity of QMI toward the HeLa cells was investigated by the methyl thiazolyl tetrazolium (MTT) assay. In the presence of various concentrations of QMI, the cell survival rate was estimated to be over 95% after incubation for 24 h, indicating its favorable biocompatibility (Fig. S26†). Then, the internalization of HMME (hematoporphyrin monomethyl ether, an exogenous porphyrin photosensitizer) was assessed by fluorescence confocal microscopy (Fig. S27†). After the incubation of cells with HMME, a distinct fluorescence characteristic was clearly observed within the cells, indicating its effective penetration of the cell membrane.

Subsequently, we validated the ability of QMI to visualize intracellular $^1O_2$ generated by internalized HMME in living cells. Specifically, cells were incubated with QMI and HMME individually or in combination in 96-well plates. Due to the absence of $^1O_2$ generation, no signals were detected in the dark groups. Similarly, groups incubated with only QMI or HMME did not emit CL signals even under light irradiation. In contrast, after being co-incubated with QMI and HMME together, an unambiguous CL signal was observed following light irradiation, suggesting that the zwitterionic probe QMI enables the sensing of intracellular $^1O_2$ in living cells (Fig. S27†).

Furthermore, we utilized the zwitterionic probe QMI to track endogenous $^1O_2$ produced during the cellular photosensitizing process. 5-Aminolevulinic acid (5-ALA), a naturally occurring amino acid, is approved by the U.S. Food and Drug Administration (FDA) for cancer diagnosis and treatment as photodynamic therapy.[56,57] It can be metabolized to the bioactive

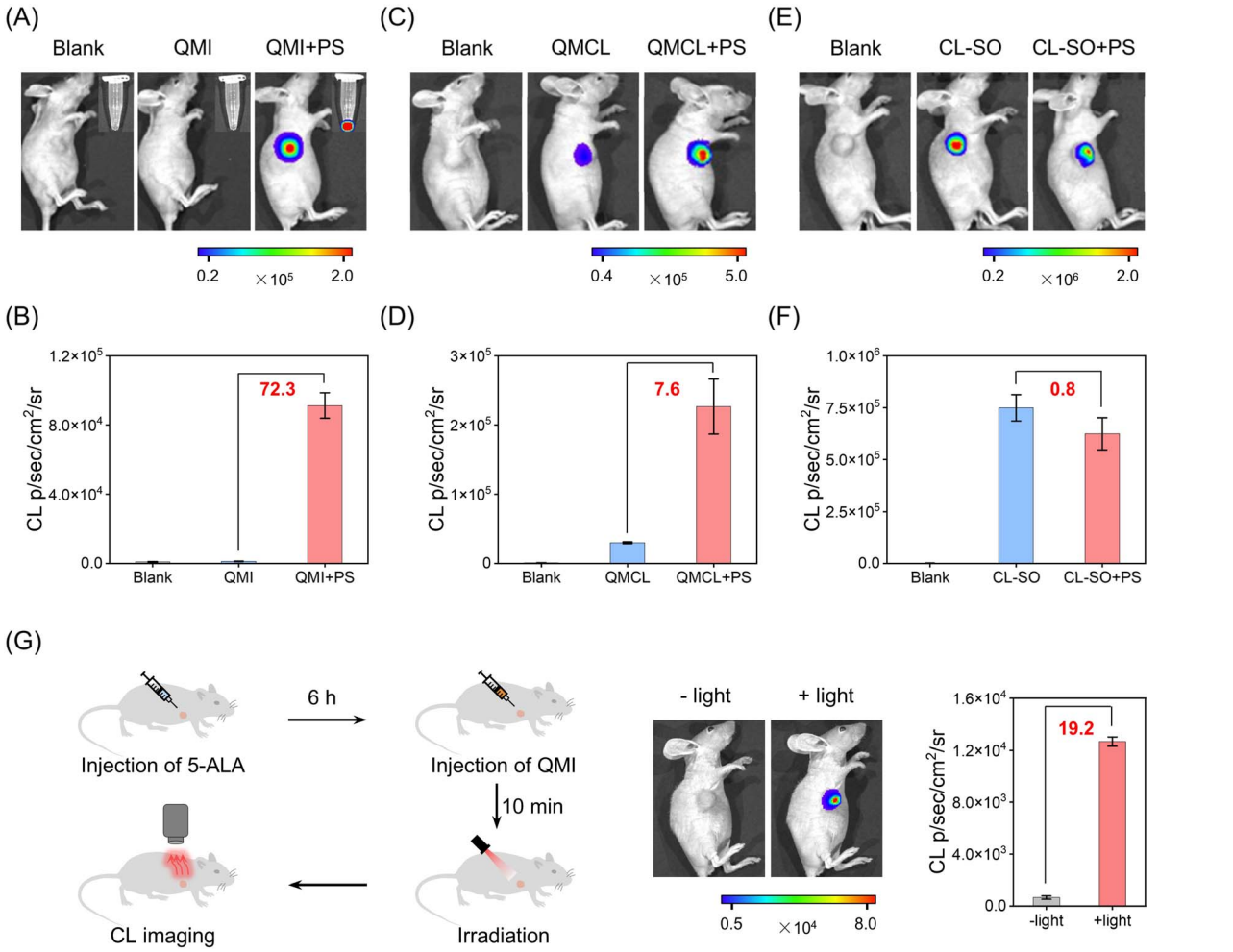

Fig. 6 *In vivo* CL imaging of intratumor $^1O_2$ during photodynamic therapy. CL images of HeLa xenograft tumor-bearing mice after intratumor injection of the zwitterionic probe QMI or QMI + PS mixed solution (A), QMCL or QMCL + PS mixed solution (C), and CL-SO or CL-SO + PS mixed solution (E). Inset: *in vitro* CL images of QMI. CL images were acquired upon white light (120 mW cm^{-2}) irradiation for 1 min. Quantification of CL signal intensities evolving from mice: zwitterionic CL probe QMI (B), QMCL (D), and CL-CO (F). (G) Schematic diagram of CL imaging of $^1O_2$ from FDA-approved 5-ALA in living mice. CL images of pretreated xenograft tumor-bearing mice. Quantification of CL signal intensities in corresponding mice. CL images were acquired upon 635 nm laser (200 mW cm^{-2}) irradiation for 3 min. Data with error bars are expressed as mean ± s.d., $n = 3$.

photosensitizer protoporphyrin IX (PpIX) through the heme biosynthesis pathway (Scheme S2†).[58] As shown in Fig. 5A, 5-ALA was initially added to HeLa cells for 24 hours to establish an endogenous PpIX cell model. Subsequently, the probe QMI was added to HeLa cells and allowed to incubate for 1 hour. Following the incubation, HeLa cells were washed three times with PBS to remove residues of 5-ALA and QMI. Finally, the CL signal from the cells was promptly collected after light irradiation. The observed characteristic fluorescence of PpIX in HeLa cells within 620–710 nm indicated the successful establishment of the endogenous PpIX cell model (Fig. 5B). As expected, a conspicuous CL signal appeared in the QMI and 5-ALA pretreatment groups after irradiation, which was a 46-fold increase compared to the corresponding dark group (Fig. 5C). In contrast, cells treated with either QMI or 5-ALA alone displayed no recognizable CL signals even under light irradiation (Fig. 5C and D). In addition, QMI only consumed a small amount of singlet oxygen; therefore, it did not affect the efficiency of 5-ALA-mediated PDT treatment (Fig. S28†). All these results provide strong support that the zwitterionic CL probe QMI successfully and effectively tracks the intracellular $^1O_2$ generation during the PDT process.

In situ monitoring of singlet oxygen from FDA-approved 5-ALA in living mice

Motivated by the excellent *in vitro* performance of the zwitterionic CL probe, we further explore the sensing capabilities of QMI for $^1O_2$ in living mice. As shown in Fig. 6A, the CL signal exhibited neglectable enhancement in the QMI-only group upon light irradiation. Notably, there was an exponential increase of approximately 72.3-fold in the chemiluminescence signal for $^1O_2$ from the co-injected group of the zwitterionic QMI and photosensitizers (rose bengal, RB) under light irradiation (Fig. 6B and S29†). In contrast, the photoactivable probe QMCL,

even without the photosensitizer, displayed a significant CL signal (31-fold enhancement) under light irradiation in living mice (Fig. 6C), due to its inherent photoinduced activation characteristic. Consequently, suffering from severely photoinduced interference, the CL enhancement of QMCL towards $^1O_2$ was limited to a modest 7.6-fold with the presence of photosensitizer (Fig. 6D). Similar photo-induced side effects were found in the previously reported CL probe CL-SO (Scheme S2†) towards $^1O_2$,[59] with the exception of a slight decrease rather than enhancement in CL signals with photosensitizer (Fig. 6E and F). These results collectively suggest that the zwitterionic strategy for QMI can effectively mitigate photo-induced side reactions and therefore enable accurate *in vivo* detection of $^1O_2$.

Furthermore, we undertook a comparison with the commercial probes SOSG and ICG, and the *in vivo* capability of the zwitterionic probe QMI to sense $^1O_2$ *in vivo* was evaluated in living mice. Notably, the fluorescence signal of SOSG in response to $^1O_2$ generated from photosensitizers was merely 1.2-fold higher under light irradiation in living mice (Fig. S30†), primarily due to its photo-induced strong background fluorescence. This slight increase was much lower than the SNR of QMI. Subsequently, we explored and validated the sensitivity of QMI in detecting $^1O_2$ during the ICG-based PDT process. A remarkably enhanced signal was observed in the QMI and ICG groups upon 808 nm laser irradiation (Fig. S31†), which could not be observed using the available probes. Indeed, the zwitterionic probe QMI possesses the capability to effectively sense even slight amounts of $^1O_2$ in living mice. Similarly, a bright CL signal was also obtained in the QMI and Cy5 groups under 635 nm laser irradiation (Fig. S32†). All these *in vivo* imaging results indicated that the zwitterionic CL probe QMI has an ultra-high sensitivity towards *in vivo* $^1O_2$.

We further investigated the practical application of QMI in PDT treatment. As shown in Fig. 6G, the FDA-approved phototherapeutic drug 5-ALA was pre-injected into the tumor for 6 h, followed by the intratumoral injection of the zwitterionic probe QMI for 10 minutes prior to light irradiation. In this context, 5-ALA serves to induce the tumor to produce endogenous PpIX for subsequent PDT, while QMI functions as an indicator, offering real-time feedback on therapeutic efficacy. Upon light irradiation, a distinct CL signal was evident in the tumor tissue, showing an approximately 19-fold enhancement. The clinical PDT results demonstrated that the zwitterionic probe QMI could efficiently identify *in vivo* $^1O_2$, thus enabling immediate feedback on PDT treatment effectiveness and guiding personalized therapy.

Conclusions

We present a *de novo* zwitterionic design strategy to construct ultra-stable NIR chemiluminescent probes, making a breakthrough in an effective solution for resolving inherent photoinduced side reactions with poor selectivity towards $^1O_2$. TD-DFT calculation and transient absorption spectroscopy confirmed that the zwitterionic CL probes undergo conversion into an inert ketone excited state with an extremely short lifetime (14 ps) through conical intersection (CI), impeding the undesirable photoreaction. Fundamentally, the ultra-stable zwitterionic strategy ensures transforming the [2 + 2] cycloaddition between the enolether unit and $^1O_2$ into a distinctive recognition process against other strong oxidative ROS. Compared with the well-known commercial probe SOSG, the zwitterionic probe QMI displays ultra-high selectivity and sensitivity (SNR over 40-fold) towards $^1O_2$. This zwitterionic chemiluminescence strategy breaks the bottlenecks of photolysis and fragility from the electron-rich enolether moiety. Of particular significance is that the zwitterionic NIR probe QMI, with excellent selectivity, high sensitivity, and outstanding photostability towards $^1O_2$, successfully monitored the FDA-approved 5-ALA-mediated *in vivo* PDT process in living mice in real time. We anticipate that this straightforward and versatile zwitterionic design strategy opens a new avenue for high-performance chemiluminescent probes, thereby contributing to the expansion of the *in vivo* toolbox.

Data availability

Experimental procedures and all relevant data are available in ESI† and from the authors.

Author contributions

All the experiments were conducted by Y. L., Y. Z., and C. Y. with the supervision of Z. G. and W. Z. All the computational work was conducted by X. W. with the supervision of X. L. All the femtosecond transient absorption spectra experiments were conducted by R. P. with the supervision of W. L. All authors discussed the results and co-wrote the manuscript.

Conflicts of interest

The authors declare no competing financial interests.

Acknowledgements

This work was supported by NSFC/China (32121005, 22225805, 22308101, and 32394001), the National Key Research and Development Program (2021YFA0910000), the Shanghai Science and Technology Innovation Action Plan (No. 23J21901600), the Innovation Program of Shanghai Municipal Education Commission, the Shanghai Frontier Science Research Base of Optogenetic Techniques for Cell Metabolism (Shanghai Municipal Education Commission, grant 2021 Sci & Tech 03-28), the China Postdoctoral Science Foundation (2021M701199), the Shanghai Municipal Science and Technology Major Project (Grant 2018SHZDZX03), and the Natural Science Foundation of Shanghai (23ZR1416600).

Notes and references

1 J.-T. Hou, K.-K. Yu, K. Sunwoo, W. Y. Kim, S. Koo, J. Wang, W. X. Ren, S. Wang, X.-Q. Yu and J. S. Kim, *Chem*, 2020, **6**, 832–866.

2 J. H. Kim, P. Verwilst, M. Won, J. Lee, J. L. Sessler, J. Han and J. S. Kim, *J. Am. Chem. Soc.*, 2021, **143**, 14115–14124.
3 H. Wu, L. Wang, Y. Wang, Y. Shao, G. Li, K. Shao and E. U. Akkaya, *Angew. Chem., Int. Ed.*, 2022, **61**, e202210249.
4 X. Wu, M. Yang, J. S. Kim, R. Wang, G. Kim, J. Ha, H. Kim, Y. Cho, K. T. Nam and J. Yoon, *Angew. Chem., Int. Ed.*, 2022, **61**, e202200808.
5 W. Chen, Z. Wang, M. Tian, G. Hong, Y. Wu, M. Sui, M. Chen, J. An, F. Song and X. Peng, *J. Am. Chem. Soc.*, 2023, **145**, 8130–8140.
6 M.-Y. Wu, L. Chen, Q. Chen, R. Hu, X. Xu, Y. Wang, J. Li, S. Feng, C. Dong, X.-L. Zhang, Z. Li, L. Wang, S. Chen and M. Gu, *Adv. Mater.*, 2022, **35**, 2208578.
7 W. Zhu, Y. Li, S. Guo, W.-J. Guo, T. Peng, H. Li, B. Liu, H.-Q. Peng and B. Z. Tang, *Nat. Commun.*, 2022, **13**, 7046.
8 X. Li, S. Yu, Y. Lee, T. Guo, N. Kwon, D. Lee, S. C. Yeom, Y. Cho, G. Kim, J.-D. Huang, S. Choi, K. T. Nam and J. Yoon, *J. Am. Chem. Soc.*, 2019, **141**, 1366–1372.
9 W. Wu, D. Mao, F. Hu, S. Xu, C. Chen, C.-J. Zhang, X. Cheng, Y. Yuan, D. Ding, D. Kong and B. Liu, *Adv. Mater.*, 2017, **29**, 1700548.
10 X. Zhao, Q. Yao, S. Long, W. Chi, Y. Yang, D. Tan, X. Liu, H. Huang, W. Sun, J. Du, J. Fan and X. Peng, *J. Am. Chem. Soc.*, 2021, **143**, 12345–12354.
11 N. Hananya, O. Green, R. Blau, R. Satchi-Fainaro and D. Shabat, *Angew. Chem., Int. Ed.*, 2017, **56**, 11793–11796.
12 L. Lei, F. Yang, X. Meng, L. Xu, P. Liang, Y. Ma, Z. Dong, Y. Wang, X.-B. Zhang and G. Song, *J. Am. Chem. Soc.*, 2023, **145**, 24386–24400.
13 B. Li, L. Lin, H. Lin and B. C. Wilson, *J. Biophotonics*, 2016, **9**, 1314–1325.
14 C. Zhao, J. Chen, R. Zhong, D. S. Chen, J. Shi and J. Song, *Angew. Chem., Int. Ed.*, 2021, **60**, 9804–9827.
15 J. Lyu, M. Cheng, J. Liu and J. Lv, *ACS Appl. Mater. Interfaces*, 2022, **14**, 54081–54089.
16 S. Chen, Y. Zhong, W. Fan, J. Xiang, G. Wang, Q. Zhou, J. Wang, Y. Geng, R. Sun, Z. Zhang, Y. Piao, J. Wang, J. Zhuo, H. Cong, H. Jiang, J. Ling, Z. Li, D. Yang, X. Yao, X. Xu, Z. Zhou, J. Tang and Y. Shen, *Nat. Biomed. Eng.*, 2021, **5**, 1019–1037.
17 N. Ruan, Q. Qiu, X. Wei, J. Liu, L. Wu, N. Jia, C. Huang and T. D. James, *J. Am. Chem. Soc.*, 2024, **146**, 2072–2079.
18 W. Zeng, L. Wu, Y. Ishigaki, T. Harimoto, Y. Hu, Y. Sun, Y. Wang, T. Suzuki, H. Y. Chen and D. Ye, *Angew. Chem., Int. Ed.*, 2022, **134**, e202111759.
19 E. M. Surender, S. J. Bradberry, S. A. Bright, C. P. McCoy, D. C. Williams and T. Gunnlaugsson, *J. Am. Chem. Soc.*, 2016, **139**, 381–388.
20 H. Shen, F. Sun, X. Zhu, J. Zhang, X. Ou, J. Zhang, C. Xu, H. H. Y. Sung, I. D. Williams, S. Chen, R. T. K. Kwok, J. W. Y. Lam, J. Sun, F. Zhang and B. Z. Tang, *J. Am. Chem. Soc.*, 2022, **144**, 15391–15402.
21 L. Wang, M. Tran, E. D'Este, J. Roberti, B. Koch, L. Xue and K. Johnsson, *Nat. Chem.*, 2020, **12**, 165–172.
22 H. Liu, P. J. H. Carter, A. C. Laan, R. Eelkema and A. G. Denkova, *Sci. Rep.*, 2019, **9**, 8393.
23 R. Ruiz-González, R. Bresolí-Obach, Ò. Gulías, M. Agut, H. Savoie, R. W. Boyle, S. Nonell and F. Giuntini, *Angew. Chem., Int. Ed.*, 2017, **56**, 2885–2888.
24 S. Kim, T. Tachikawa, M. Fujitsuka and T. Majima, *J. Am. Chem. Soc.*, 2014, **136**, 11707–11715.
25 A. Gollmer, J. Arnbjerg, F. H. Blaikie, B. W. Pedersen, T. Breitenbach, K. Daasbjerg, M. Glasius and P. R. Ogilby, *Photochem. Photobiol.*, 2011, **87**, 671–679.
26 X. Su, X. Kong, K. Sun, Q. Liu, Y. Pei, D. Hu, M. Xu, W. Feng and F. Li, *Angew. Chem., Int. Ed.*, 2022, **61**, e202201630.
27 C. Chen, H. Gao, H. Ou, R. T. K. Kwok, Y. Tang, D. Zheng and D. Ding, *J. Am. Chem. Soc.*, 2022, **144**, 3429–3441.
28 Y. Liu, L. Teng, Y. Lyu, G. Song, X.-B. Zhang and W. Tan, *Nat. Commun.*, 2022, **13**, 2216.
29 J. Cao, W. An, A. G. Reeves and A. R. Lippert, *Chem. Sci.*, 2018, **9**, 2552–2558.
30 T. E. Anderson, A. A. Andia and K. A. Woerpel, *Tetrahedron*, 2021, **82**, 131874.
31 J. A. Bull, R. A. Croft, O. A. Davis, R. Doran and K. F. Morgan, *Chem. Rev.*, 2016, **116**, 12150–12233.
32 B. Yang and Z. Lu, *J. Org. Chem.*, 2016, **81**, 7288–7300.
33 J. Huang, L. Su, C. Xu, X. Ge, R. Zhang, J. Song and K. Pu, *Nat. Mater.*, 2023, **22**, 1421–1429.
34 Y. Zhang, C. Yan, C. Wang, Z. Guo, X. Liu and W.-H. Zhu, *Angew. Chem., Int. Ed.*, 2020, **59**, 9059–9066.
35 C. Li, Y. Xu, L. Tu, M. Choi, Y. Fan, X. Chen, J. L. Sessler, J. S. Kim and Y. Sun, *Chem. Sci.*, 2022, **13**, 6541–6549.
36 Q. Xu, Y. Zhang, M. Zhu, C. Yan, W. Mao, W.-H. Zhu and Z. Guo, *Chem. Sci.*, 2023, **14**, 4091–4101.
37 L. Wu, J. Liu, P. Li, B. Tang and T. D. James, *Chem. Soc. Rev.*, 2021, **50**, 702–734.
38 W. Zhang, Y. Lv, F. Huo, Y. Yun and C. Yin, *Adv. Mater.*, 2024, 2314021.
39 X. Wei, J. Huang, C. Zhang, C. Xu, K. Pu and Y. Zhang, *Angew. Chem., Int. Ed.*, 2023, **62**, e202213791.
40 L. A. MacManus-Spencer and K. McNeill, *J. Am. Chem. Soc.*, 2005, **127**, 8954–8955.
41 S. Gutkin, R. Tannous, Q. Jaber, M. Fridman and D. Shabat, *Chem. Sci.*, 2023, **14**, 6953–6962.
42 Y. Danten, C. Gatti and C. Frayret, *J. Phys. Chem. A*, 2022, **126**, 9577–9593.
43 K. Kajiwara, H. Osaki, S. Greßies, K. Kuwata, J. H. Kim, T. Gensch, Y. Sato, F. Glorius, S. Yamaguchi and M. Taki, *Nat. Commun.*, 2022, **13**, 2533.
44 Z. Guo, C. Yan and W.-H. Zhu, *Angew. Chem., Int. Ed.*, 2020, **59**, 9812–9825.
45 M. Hao, W. Chi, C. Wang, Z. Xu, Z. Li and X. Liu, *J. Phys. Chem. C*, 2020, **124**, 16820–16826.
46 A. Kahan, A. Wand, S. Ruhman, S. Zilberg and Y. Haas, *J. Phys. Chem. A*, 2011, **115**, 10854–10861.
47 L. Shi, C. Yan, Z. Guo, W. Chi, J. Wei, W. Liu, X. Liu, H. Tian and W.-H. Zhu, *Nat. Commun.*, 2020, **11**, 793.
48 Y.-L. Lee, Y.-T. Chou, B.-K. Su, C.-c. Wu, C.-H. Wang, K.-H. Chang, J.-a. A. Ho and P.-T. Chou, *J. Am. Chem. Soc.*, 2022, **144**, 17249–17260.
49 Y. You, *Org. Biomol. Chem.*, 2018, **16**, 4044–4060.

50 M. A. Filatov, S. Karuthedath, P. M. Polestshuk, H. Savoie, K. J. Flanagan, C. Sy, E. Sitte, M. Telitchko, F. Laquai, R. W. Boyle and M. O. Senge, *J. Am. Chem. Soc.*, 2017, **139**, 6282–6285.
51 T. Luo, Q. Zhang and Q.-B. Lu, *Cancers*, 2017, **9**, 63.
52 C. Shirata, J. Kaneko, Y. Inagaki, T. Kokudo, M. Sato, S. Kiritani, N. Akamatsu, J. Arita, Y. Sakamoto, K. Hasegawa and N. Kokudo, *Sci. Rep.*, 2017, **7**, 13958.
53 J. Atchison, S. Kamila, H. Nesbitt, K. A. Logan, D. M. Nicholas, C. Fowley, J. Davis, B. Callan, A. P. McHale and J. F. Callan, *Chem. Commun.*, 2017, **53**, 2009–2012.
54 R. H. Kang, Y. Kim, H. J. Um, J. Kim, E.-K. Bang, S. G. Yeo and D. Kim, *ACS Appl. Nano Mater.*, 2022, **5**, 5387–5397.
55 S. Joseph and S. K. Ashok Kumar, *Coord. Chem. Rev.*, 2023, **496**, 215408.
56 K. Mahmoudi, K. L. Garvey, A. Bouras, G. Cramer, H. Stepp, J. G. Jesu Raj, D. Bozec, T. M. Busch and C. G. Hadjipanayis, *J. Neuro-Oncol.*, 2019, **141**, 595–607.
57 L. Marocco, F. Umrath, S. Sachsenmaier, R. Rabiner, N. Wülker and M. Danalache, *Biomedicines*, 2022, **10**, 2900.
58 Y. Shinoda, D. Kato, R. Ando, H. Endo, T. Takahashi, Y. Tsuneoka and Y. Fujiwara, *Pharmaceuticals*, 2021, **14**, 229.
59 M. Yang, J. Zhang, D. Shabat, J. Fan and X. Peng, *ACS Sens.*, 2020, **5**, 3158–3164.